Force-Controlled Mechanical Stimulation and Single-Neuron Fluorescence Imaging of *Drosophila* Larvae

Weize Zhang, *Student Member, IEEE*, Peng Pan, *Student Member, IEEE*, Xin Wang, *Member, IEEE*, Yixu Chen, Yong Rao, and Xinyu Liu, *Member, IEEE*

***Abstract*—Studying the neural response of a *Drosophila* larva to touch stimulation could decipher neural basis of the creature's danger-escaping behaviors. This letter reports force-controlled robotic mechanical stimulation and single-neuron fluorescence imaging of *Drosophila* larvae. A force control architecture based on a model compensation-prediction scheme and a switched fuzzy-PID controller was used for regulating the touch force applied to a larva at the micronewton level. The developed force control system demonstrates a settling time of 0.15 s, zero overshoot and a resolution of <50 μN. Established based on a high-resolution inverted fluorescence microscope, our robotic system is capable of simultaneously applying a controlled touch force to a larva and quantifying the fluorescence signal transmission inside a single neuron responsive to body touch stimulation. Using this system, we examined, for the first time, the quantitative relationship between the applied force level (range: 0.25–2 mN) and the change in transmission signal of the class III ddaA neuron. The touch force threshold at which the neuron starts to get activated was determined to be in the range of 0.25–0.5 mN. This work may contribute to new studies on sensory mechanotransduction in *Drosophila* larvae.**

***Index Terms*—Robotic micromanipulation, force sensing and control, calcium imaging, mechanotransduction, *Drosophila* larva.**

I. Introduction

THE sense of mechanical stimulation is the basis of danger-escaping behaviors and is critical for a creature to survive. *Drosophila* larva is a common biological model for studying neural mechanisms governing its behavior-level responses to external stimulation. For instance, a *Drosophila* larva tends to turn/roll upon a touch stimulus [1]–[4]. Increasing interests arise in sensory mechanotransduction and the underlying neuronal mechanisms of *Drosophila* larvae. Even though functions of most neuron types found in the *Drosophila* larval body walls remain unexplored [2], it has been investigated that class I to IV neurons are nociceptive and related to larval locomotion, among which the class III ddaA neurons contribute to the larva response to gentle touches and can be activated by a touch force [2].

The neuronal calcium signal is a good indictor of neuron signal transmission, which can be imaged through fluorescence imaging [5]. The activities of many neurons of *Drosophila* larvae can be influenced by different environmental factors [4], [6]–[8], among which the activities of class III ddaA neurons of certain genotypes have been found to strongly correlate with mechanical stimulation applied to the larva body [2]. One common method to investigate this correlation is to visualize the change in calcium fluorescence intensity of single neurons upon mechanical stimulation of the larva body. Previous studies have confirmed this phenomenon with a constant force applied to the larval body. In [2], [9], experiments were performed at the force level of 1 mN, and the time history of fluorescence intensity of the neuronal calcium signal was recorded. The class III ddaA neuron was found to have significant changes in the calcium fluorescence intensity upon larva body touch [2].

Despite the previous results with great promise for mechanotransduction studies of *Drosophila* larvae [2], [9], these experiments were performed with a fixed force level and the force measurement method (by visually measuring the deflection of an eyelash or fiber touching the larva) [1] introduced relatively large errors compared to the use of an accurate force sensor [10], [11]. In addition, it is intuitive to speculate that there exists a quantitative relationship between the touch force level and the calcium fluorescence intensity of the class III ddaA neurons in *Drosophila* larva; however, due to the lack of accurate force measurement and control in the previous experimental setup, this relationship has not been quantified.

In the last decade, because of their unique advantages like high manipulation speed and precision, robotic biomanipulation systems have been widely used in many biological applications such as cell mechanics [12]–[14], cell transportation [15]–[17], grasping [18]–[21], orientation [22], [23], transgenic animal production [24]–[26], drug screening [27], disease study [28],

Manuscript received December 12, 2020; accepted February 6, 2021. Date of publication February 24, 2021; date of current version March 29, 2021. This letter was recommended for publication by Associate Editor J. Cortes and Editor N. Amato upon evaluation of the reviewers' comments. This work was supported by the National Sciences and Engineering Research Council of Canada under Grant RGPIN-2017-06374 and Grant RGPAS 2017-507980. *(Weize Zhang and Peng Pan contributed equally to this work.) (Corresponding author: Xinyu Liu.)*

Weize Zhang is with the Department of Mechanical Engineering, McGill University, Montreal H3A 0C3, Quebec, Canada (e-mail: weize.zhang@mail.mcgill.ca).

Peng Pan and Xinyu Liu are with the Department of Mechanical and Industrial Engineering, University of Toronto, Toronto M5S3G8, Ontario, Canada, and also with the Department of Mechanical Engineering, McGill University, Montreal H3A 0C3, Quebec, Canada (e-mail: peng.pan@mail.mcgill.ca; xyliu@mie.utoronto.ca).

Xin Wang is with the Department of Mechanical and Aerospace Engineering, Jilin University, Changchun 130012, China (e-mail: wangxin_jlu@jlu.edu.cn).

Yixu Chen and Yong Rao are with the Department of Neurology and Neurosurgery, McGill University, Montreal H3A 2B4, Quebec, Canada (e-mail: yixu.chen@mail.mcgill.ca; yong.rao@mcgill.ca).

Digital Object Identifier 10.1109/LRA.2021.3061874

[29], and in-vitro fertilization [30]. Recently, we have developed a force-controlled robotic system capable of simultaneous mechanical stimulation and calcium fluorescence imaging on *Drosophila* larvae [31], and also proposed new force control approaches for improving the system's force control performance [32], [33]. Using the system, we have demonstrated fluorescence imaging on groups of multiple neurons at different touch force levels [31]. One limitation of this system is its relatively low imaging resolution because of the stereo fluorescence microscope employed, which prevents us from single-neuron fluorescence imaging.

To better understand the mechanotransduction mechanism of *Drosophila* larvae, it is necessary to observe fluorescence signal change at single neuron resolution. In this letter, we replaced the stereotype microscope with an inverted microscope for single-neuron fluorescence imaging. Compared to our previous system [31], the adoption of an inverted microscope raises several technical challenges such as the small field of view (FOV) and the constrained microscope workspace, requiring the robotic manipulation strategy to be significantly revised (see Section II-B).

This work aims to extend our robotic micromanipulation system to simultaneous force-controlled larva touching and single-neuron fluorescence imaging on *Drosophila* larvae. We redesigned our system based on an inverted fluorescence microscope and revised the entire larva manipulation strategy to accommodate the characteristics of the inverted microscope. Furthermore, we developed an advanced force controller to regulate the touch force applied to the larva body, which combines two force control strategies we previously developed separately: a compensation-prediction scheme [33] and a switched fuzzy-PID control [32]. It was demonstrated that the new controller possesses improved dynamic performance over each individual method. We performed touch stimulation experiments on a *Drosophila* genotype with fluorescent class III ddaA neurons and quantified their changes in calcium fluorescence intensity at different force levels. Our results provide, for the first time, the quantitative relationship between the calcium signal change of class III ddaA neurons and the touch force level applied to a *Drosophila* larva, based on which the minimum force level at which the class III ddaA neurons of a *Drosophila* larva start to respond was determined.

II. System Architecture

A. Robotic System Setup

The setup of the robotic micromanipulation system is shown in Fig. 1. An inverted fluorescence microscope (IX-83, Olympus) was used with 4×, 10× and 20× objectives, and could switch between different objectives with a motorized turret. A high-speed fluorescence camera (Zyla, Andor) was mounted to the end of an optical spitter (OPTALSPLIT II, Cairn). The microscope and the camera together are capable of capturing high-resolution fluorescence images of single class III ddaA neurons at 8 fps. The optical splitter was responsible for splitting the output light beam of the fluorescence image into two wavelengths corresponding to the GFP (509 nm) and RFP (583 nm)

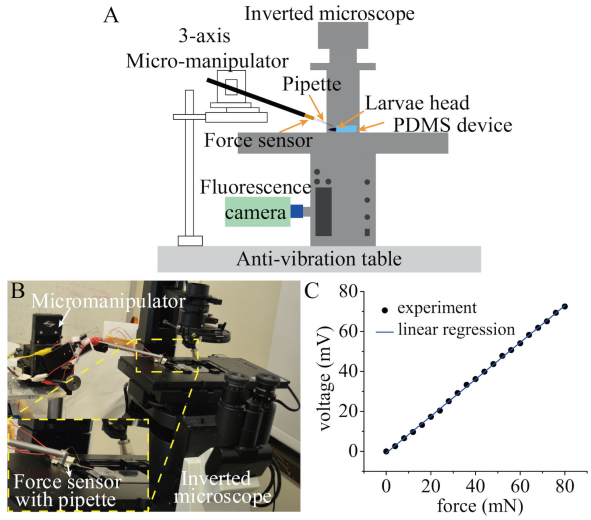

Fig. 1. (a) Schematic of the micromanipulation system. (b) Experimental setup of the micromanipulation system. (c) Calibration curve of the sensor/pipette assembly.

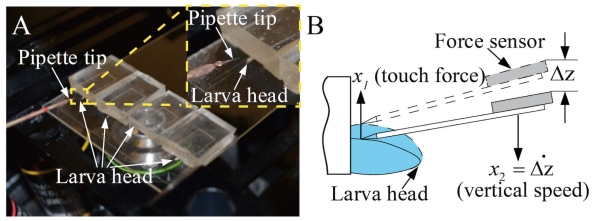

Fig. 2. (a) photograph of four larva samples immobilized by PDMS devices. (b) Schematic of the control system model.

signals emitted from the same neuron. A polydimethylsiloxane (PDMS) device with a 130 μm high channel was used to immobilize a larva onto a glass slide (covered with a double-sided adhesive tape) with its head exposed outside for touch stimulation, and the larva body was compressed by the PDMS device to be ~130 μm thin for high-resolution fluorescence imaging [31]. When larvae were fixed to glass slide by PDMS device and tape, they experienced the harsh compression stimulus by the device. However, class III ddaA neuron is used to sense the gentle touch rather than harsh compression which should be sensed by the Class IV ddaA neuron. Thus, in our experiments the influence of the compression force between a larva, the PDMS device and the tape on class III ddaA neuron response is small.

Each sample slide contains four immobilized larvae and mounted on the motorized XY stage of the microscope [Fig. 2(a)]. A glass pipette was used as the end-effector for larvae touching, and was glued onto a piezoresistive force sensor (AE801, Sensor). The pipette-sensor assembly was attached to a steel holder and then mounted onto a three-degree-of-freedom (3-DOF) micromanipulator (MP-285, Sutter). The force sensor output was read out through a Wheatstone bridge circuit and acquired with a data acquisition board (USB 6343, National Instruments). To calibrate the sensor/pipette assembly, a precision balance (MXX-123, Denver Instrument; force resolution: 10 μN) was used. After vertically touching the balance, readings of balance and corresponding output voltages of the Wheatstone

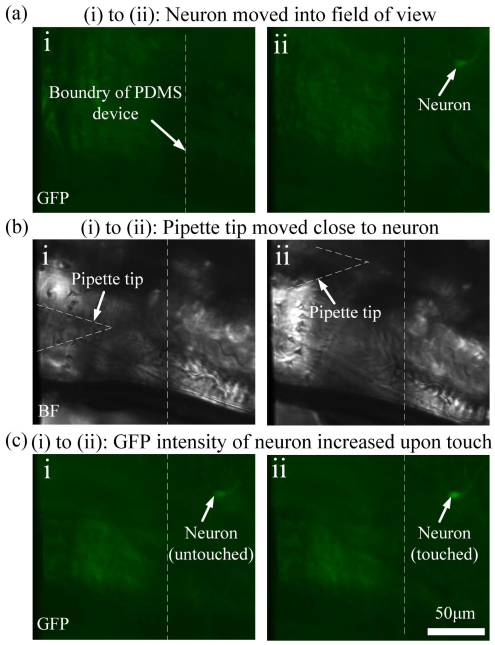

Fig. 3. System operation steps. (a) Positioning of an identified neuron to the FOV under the GFP fluorescent mode. (i) and (ii) Before and after the neuron positioning. (b) Positioning of the pipette tip (labelled by dashed line) to the proximity of the identified neuron under the bright-field (BF) mode. (i) and (ii) Before and after the pipette positioning. (c) Closed-loop controlled touch stimulation of the larvae tissue and fluorescence imaging of the identified neuron. (i) and (ii) Before and after stimulation.

bridge circuit were recorded. The calibration data are plotted in the Fig. 1(c). The measurement range, resolution and sensitivity of the sensor/pipette assembly were determined to be 0–80 mN, 50 μN, and 0.93 mV/mN, respectively. Fig. 2(b) is the schematic of a simplified mechanical model of lava touching with the assumption of linear elasticity of the larva body. Note that the horizonal component of the touch force can be safely ignored because the larva body surface where we apply the touch force is approximately flat after the body was compressed by the PDMS device.

B. System Operation Procedure

Different from our previous system [31], the system here employs an inverted microscope and a faster and more sensitive fluorescence camera to quantify the calcium fluorescence signals from single neurons of the larva. Note that the touch stimulation of a single neuron requires that the pipette tip and the neuron to be in the same FOV under 20× magnification [2]. Thus, we must stimulate and observe the neurons immobilized within the PDMS device but close to the device side wall [see Fig. 3(a)-ii]. In our previous setup [31], the automated larva touch manipulation was performed under a stereo microscope with a 4× objective, and thus could not quantify fluorescence signals of a single neuron. In this work, the system is operated through teleoperation by a user sitting in front of a computer screen. The system allows an operator to perform all the operation steps under a 20× objective via keyboard inputs.

Before each experiment, the assembly of glass pipette and force sensor is mounted on the micromanipulator. The initial in-plane position (in the image coordinate frame) of glass pipette tip is set in the left side of FOV which is close to but not overlapped with the area where the PDMS wall would be placed. The initial out-of-plane position of the glass pipette tip is set to make the pipette tip visible in the FOV under bright field mode and high enough to avoid the collision with the larvae body (body height:$\sim$1.2 mm). To start an experiment, a larva is immobilized on the glass slide using PDMS device with its head towards to the glass pipette tip. The control sequence starts with locating the initial position of glass pipette. The initial in-plane and out-of-plane coordinates of the pipette tip in the coordinate frame of micromanipulator are recorded by reading the coordinates of micromanipulator along each axis. The initial position of the glass pipette is set as its home position, to which the glass pipette would be brought back after performing manipulation and imaging of each target larva.

Fig. 3 illustrates the rest steps of control sequence in details. Once the initial position of glass pipette is determined, the following step is to move the identified neuron to the FOV under the fluorescence mode (magnification: 20×), as shown in Fig. 3(a)-ii. Then, the system switches to the bright field mode [Fig. 3(b)-i] and the operator moves the pipette tip to the vicinity of the neuron via keyboard control [Fig. 3(b)-ii]. Note that, under 20× bright field illumination, the pipette tip is not completely clear but still discernible [indicated by the dashed lines in Fig. 3(b)]. After that, the system switches back to the fluorescence mode, and a closed-loop controlled touch force is applied to the larva and the fluorescence images recorded simultaneously.

One reason for having these specific operation steps is that the non-fluorescent pipette tip is not observable in the fluorescence mode. To make sure the pipette tip and the neuron are both in the same FOV under 20×, the system switches to the bright field mode [from Figs. 3(a)-ii to 3(b)-i] to visualize the pipette tip and make sure it does not contact the side wall of the PDMS device [indicated by the vertical dashed line in Fig. 3]. The pipette tip is blocked by the larval body and is out of focus, making its image blurred but still visible in the bright field mode. In Figs. 3(b)-i and 3(b)-ii, one can see that the pipette tip is on the left side of the device side wall, which does not contact the PDMS device and could be moved freely. The neuron is on the right side of the device side wall and is immobilized inside the channel.

III. Force Controller Design and Validation

A. System Modeling

We developed an advanced force controller with fast dynamics for regularting the contact force during larva touching, which integrate a switched fuzzy-PID control law [32] and a compensation-prediction scheme [33]. The switched fuzzy-PID control law [32] achieved significantly improved system dynamics, and the compensation-prediction controller scheme was capable of readily handling unknown model errors, system time delay, and force feedback noise. The combination of these two control methods further improves the system dynamics over each individual method, which will be shown in this section.

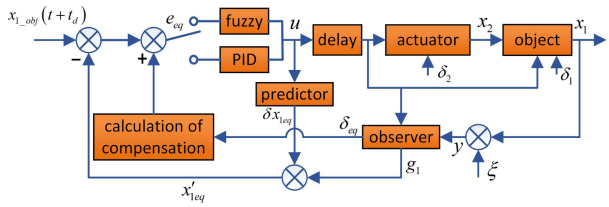

Fig. 4. Control system architecture.

To make this letter self-contained, we briefly introduce the force controller below.

The larva touching system is modeled as a two-dimensional (2D) state-space model:

$$\begin{cases} \dot{x}_1 = Kx_2 + \delta_1 \\ \dot{x}_2 = \frac{1}{T_m}\left\{H\left[u\left(t-t_d\right)\right] - x_2\right\} + \delta_2 \\ y = x_1 + \xi \end{cases} \tag{1}$$

where the variables x_1 and x_2 represent the contact force (the variable to be controlled) and the vertical speed of the micromanipulator, respectively, as shown in Fig. 2(b). The first equation is the time derivative of a linear spring touch model [32], [33], where K is the spring constant. The second equation is a time-delayed first-order dynamic model of the micromanipulator, where T_m is the time constant of the model, and $H(u)$ is the calibrated mapping function of maximum z-axis speed vs. input voltage of the micromanipulator [33]. The parameters were experimentally determined to be $K = 200$ N/m, $T_m = 0.01$ s, and $t_d = 0.05$ s [33].

B. Controller Architecture

As shown in Fig. 4, the z-axis of the micromanipulator could be treated as a first-order actuator. The system is time delayed by t_d due to the dynamics of the micromanipulator and other delay times of the system (e.g., delays of command transmission and the mechanical backlash). The system output is x_1, and its objective (reference) value is denoted by x_{1_obj}. Note that only step inputs were used for control performance validation, as they mimic sudden mechanical stimuli applied to the larva [2], [9].

The tracking error of x_1 is denoted by $e_1(t) = x_{1\_obj}(t + t_d) - x_1(t)$. Note that we use $x_{1\_obj}(t + t_d)$ instead of $x_{1\_obj}(t)$ as reference to highlight the fact that the time-delayed system will always respond to an step input with a time delay of t_d. The system has two unknown modeling errors (δ_1 and δ_2) in the two differential equations of the 2D state-space model (Equation 1). These errors are supposed to be time-varying. To make the system observable from the single force feedback loop, we combine them into an equivalent modeling error (δ_{eq}) through mathematical transformation, and then estimate δ_{eq} using a modified EHGO insensitive to the force measurement noise (ξ). The EHGO also provides a denoised value (g_1) of the force measurement y. A Smith predictor is implemented to calculate a correction (δx_{1eq}) to the tracking error caused by the system time delay. Based on the estimation (δ_{eq}) of the equivalent modeling error, a compensation is added to further correct the tracking error, and the corrected error (e_{eq}) is then injected into a controller to calculate the control input u. The selection of controller is summarized as follows: once the force command is set, the system employs the fuzzy controller first to take advantage of its fast converging speed. Since the fuzzy controller is not model dependant, it does not need any modification compared to [32]. Once the tracking error reaches a threshold of 13.6% [32], the system switches to PID controller with optimized PID ($K_p = 150$, $K_I = 200$ and $K_d = 2$) [33] under the compensation-prediction scheme.

The controller design is summarized as follows. For simplicity, we mark $\upsilon(t) = H[u(t)]$. A noise-insensitive EHGO [33] is firstly adopted to calculate an equivalent modeling error δ_{eq} and an estimation of the time-derivative of x_1:

$$\begin{cases} \dot{\hat{x}}_1 = K\hat{x}_{2eq} + \hat{\delta}_{eq} - \frac{k_1}{\varepsilon}\left(\hat{x}_1 - g_1\right) \\ \dot{\hat{x}}_{2eq} = \frac{1}{T_m}\left[\upsilon(t-t_d) - \hat{x}_{2eq}\right] - \frac{k_2}{\varepsilon^2}\left(\hat{x}_1 - g_1\right) \\ \dot{\hat{\delta}}_{eq} = -\frac{k_3}{\varepsilon^3}\left(\hat{x}_1 - g_1\right) \\ \dot{g}_1 = g_2 \\ \dot{g}_2 = g_3 \\ \dot{g}_3 = \frac{1}{\alpha^3}h\left(g_1 - y, \alpha g_2, \alpha^2 g_3\right) \end{cases} \tag{2}$$

The parameters are $k_1 = 50, k_2 = 1000, \varepsilon = 0.1, \alpha = 0.04$, and $x_{2eq} = x_2 - T_m\delta_{22}$, where $\delta_{22} = \frac{1}{T_m}e^{-\frac{t}{T_m}}\int_0^t \delta_2 e^{\frac{\tau}{T_m}}d\tau$ [33]. $h(x)$ used in this research is [34]:

$$h\left(g_1 - y, \alpha g_2, \alpha^2 g_3\right) = -4\cdot 2^{\frac{3}{5}}\left(g_1 - y + (\alpha g_2)^{\frac{9}{7}}\right)^{\frac{1}{3}} - 4\cdot\left(\alpha^2 g_3\right)^{\frac{3}{5}} \tag{3}$$

Then a traditional Smith predictor is implemented as if the system is devoid of modeling errors [33]:

$$\begin{cases} \dot{\hat{x}}_{1eq\_f} = a\hat{x}_{1eq\_f} + b\hat{x}_{2eq\_f} + cu \\ \dot{\hat{x}}_{2eq\_f} = \frac{1}{T_m}\left(\upsilon - \hat{x}_{2eq\_f}\right) \end{cases} \tag{4}$$

$$\begin{cases} \dot{\hat{x}}_{1eq} = a\hat{x}_{1eq} + b\hat{x}_{2eq} + cu(t-t_d) \\ \dot{\hat{x}}_{2eq} = \frac{1}{T_m}\left[\upsilon(t-t_d) - \hat{x}_{2eq}\right] \end{cases} \tag{5}$$

$$\delta x_{1eq} = \hat{x}_{1eq\_f} - \hat{x}_{1eq} \tag{6}$$

where $\hat{x}_{1eq}$ and $\hat{x}_{1eq\_f}$ are the estimations of x_{1eq} with and without dead time. The term δx_{1eq} is a traditional Smith predictor correction. A conventional tracking error with Smith predictor correction is

$$e_{eq} = x_{1\_obj} - (x_1 + \delta x_{1eq}) \tag{7}$$

However, given the presence of modeling errors, a compensation-prediction scheme is adopted to further rectify e_{eq}. According to discussions in [33], the compensation-prediction scheme is equivalent to implementing a Smith predictor as if we had the precise model, except for adding a supplementary correction of $e^{at}\int_0^t \delta_{eq}e^{-a\tau}d\tau - e^{a(t+t_d)}\int_0^{t+t_d}\delta_{eq}e^{-a\tau}d\tau$ to compensate for the modeling error (which corresponds to the "calculation of compensation" block in Fig. 4). The tracking error injected into the controller is:

$$e_{eq} = x_{1\_obj} - (x_1 + \delta x_{1eq}) + e^{at}\int_0^t \delta_{eq}e^{-a\tau}d\tau - e^{a(t+t_d)}\int_0^{t+t_d}\delta_{eq}e^{-a\tau}d\tau \tag{8}$$

This concludes the compensation-prediction scheme. It treats modeling errors, time delay, measurement noise and insufficient

feedback altogether. The next step is to inject the equivalent tracking error e_{eq} into an appropriate controller. Two controllers are used for at different stages of the system response: the fuzzy controller and the PID controller. The use of these two controllers are summarized as follows.

When e_{eq} is higher than a threshold set by user [32], e_{eq} and its time-derivative $\dot{e}_{eq}$ (calculated with the method described in [33]) are evaluated with a fuzzy logic lookup table, from "positive big" (PB) to "negative big" (NB). Then a fuzzy control input is derived from the lookup table consisting 56 control rules [32]:

$$\bar{v}(\tau) = \bar{v}_1(\tau) + \bar{v}_2(\tau) + \bar{v}_3(\tau) + \cdots + \bar{v}_{56}(\tau) \tag{9}$$

Finally, a numerical control input is calculated from centroid defuzzification method [32]:

$$v = v_F = \frac{\int_{-6}^{6} \bar{v}(\tau)\tau d\tau}{\int_{-6}^{6} \bar{v}(\tau) d\tau} \tag{10}$$

When e_{eq} is inferior to the threshold, a conventional PID controller is used, whose parameters are inherited from [33]:

$$v = v_{PID} = K_p e_{eq} + K_I \int e_{eq} dt + K_d \dot{e}_{eq} \tag{11}$$

Note that v is virtual input due to the nonlinear relationship between the real input u and the maximum vertical speed $H(u)$. The real input u is derived from an inversion $u = H^{-1}(v)$.

C. Force Control Performance Validation

To demonstrate the advantage of this advanced force controller, its step response was compared with those of the switched fuzzy-PID controller and a regular PID controller with the compensation-prediction scheme (denoted as "compensation-prediction + PID"). Note that the step-response data of the switched fuzzy-PID controller are not the same as these reported in [32], because a new signal readout circuit of the force sensor with electromagnetic shielding and output signal amplification has been implemented [33]. The step-response results are shown in Fig. 5. Comparing the "compensation-prediction + PID" data and the "switched fuzzy-PID" data, one can clearly see the advantage of the fuzzy controller: the logic of the fuzzy controller always tries to converge at its maximum speed [32], resulting in shorter raising time and shorter settling time. However, the performance of the switched fuzzy-PID controller still has room to improve after the switch from fuzzy to PID control. This is because when the control loop becomes model-dependent after the switch, a more accurate model with smaller modeling errors allows the observer to provide faster estimation [33]. Combining the "compensation-prediction+PID" scheme with the fuzzy controller to form a complete switched fuzzy-PID controller with the compensation-prediction scheme (denoted as "compensation-prediction+switched fuzzy-PID"), the settling time further reduces to 0.15 s without overshoot and the force control resolution is lower than 50 μN. Compared to the switched fuzzy-PID controller, our newly-proposed force controller has the same initial convergence speed, but converges faster after the controller switch, which is attributed to the compensation-prediction scheme. Compared to the regular PID controller with the compensation-prediction scheme, this new force controller displays a faster initial convergence speed due to the initial operation of the fuzzy controller.

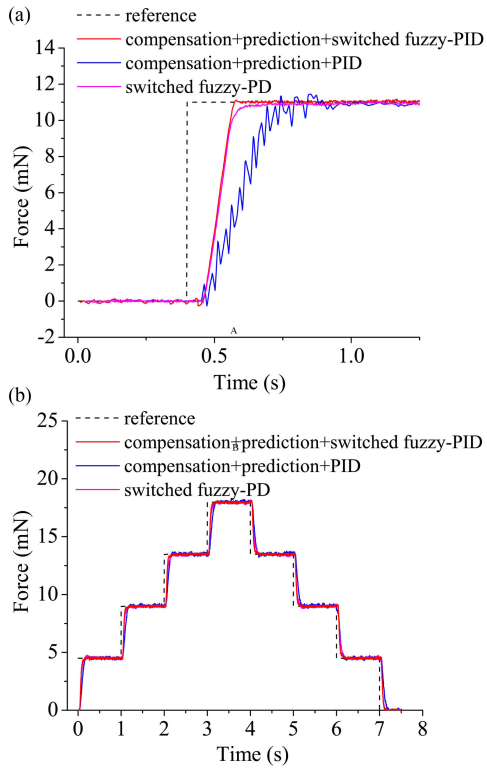

Fig. 5. Comparison of force control results from three control architectures. By combing two the compensation-prediction scheme and the switched fuzzy-PID controller, the system inherits the fast convergence characteristic of fuzzy controller before reaching the switching threshold, and converge faster than the PD controller after reaching the switching threshold. (a) Single step response. (b) Multi-step response.

IV. Drosophila Larva Preparation

NOMPC (No mechanoreceptor potential C) is a mechanotransduction channel subunit for gentle-touch sensation [9], and class III ddaA dendritic arborization neurons respond to gentle-touch sensation. NOMPC is highly expressed in class III dendritic arborization neurons, but not in other classes [2]. class III ddaA neurons in the experimental group should display significant change in calcium singal upon mechanical stimulation, whose quantitative relationship will be determined. In contrast, class III ddaA neurons of larvae in the control group should display no significant change in calcium signal [2], [9].

3rd instar *Drosophila* larvae are larvae close sexual maturity. Their size, shape and neuron network make them ideal test subjects for mechanotransduction studies [35]–[38]. We chose 3rd instar $nompC^1/nompC^3$, UAS-$nompC$/CyO, weep; GAL4 [19-12]/UAS-GCaMP6 (nompC rescue) as the genotype of the experimental group, and 3rd instar GAL4 [19-12]/UAS-GCaMP6 as the control group [9]. All the class III ddaA neurons express a genetically encoded calcium reporter, GCaMP6, and a calcium insensitive protein, red fluorescence protein (RFP). The RFP signal was used as a reference to eliminate any imaging condition variation.

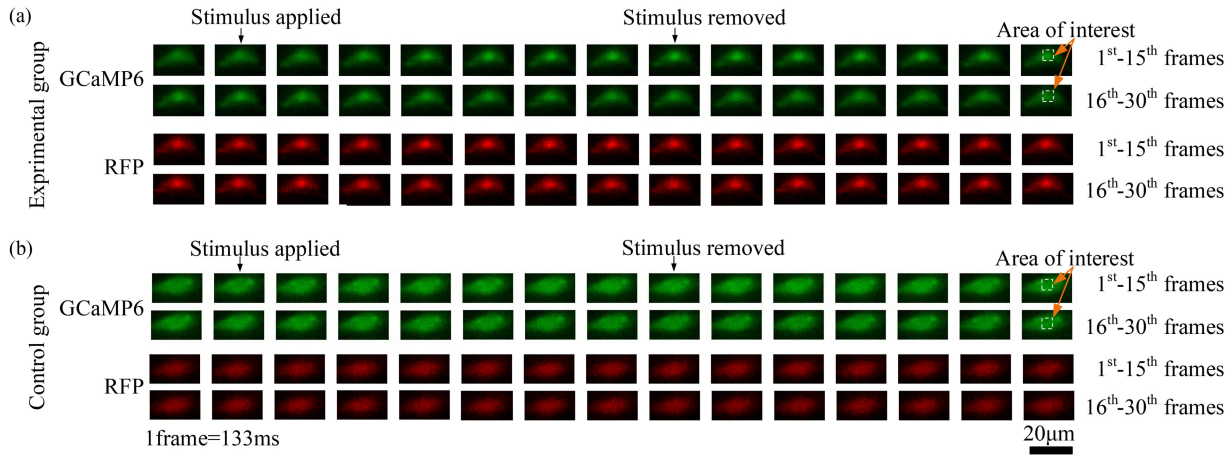

Fig. 6. Image sequences of the GCaMP6 and RFP signals from class III ddaA neurons on two larvae, one from the experimental group (a) and one from the control group (b), during and after applying a mechanical stimulus.

The larva genotypes in the experimental and control groups were produced through crossing based on four larvae lines: line 1–$nompC^3$,UAS-$nompC$; GAL4[19-12], line 2–$nompC^1$/CyO,weep; UAS-GCaMP6, line 3–GAL4 [19-12], and line 4–UAS-GCaMP6. Line 1 and line 2 were crossed for the experimental group, and line 3 and line 4 were crossed for the control group. Original larvae lines were raised in *Drosophila* agar with apple juice under room temperature. The number of eggs were limited to $\leq$200 per dish. It took 11–12 days for the larva eggs to develop from embryo, 1st-3rd instar larva, and pupa stages, and adults eventually emerged from the pupae. Immediately after the eclosion, virgin larvae were picked out for crossing to minimize the possibility of mutated gene. The offsprings were kept in the same *Drosophila* agar.

V. Experimental Results and Discussion

We first applied a touch force of 1 mN to one class III ddaA neuron five times and observed the changes in fluorescence intensity of the neuron. This was to verify whether the response to touch is repeatable. Then, we applied touch forces at 2 mN, 1 mN, 0.5 mN and 0.25 mN to larvae from the experimental group. Each force level was applied for 30 times on three larvae (two neurons per larva, five times of stimulation per force level, and thus 10 sets of fluorescence signal data per larva). This was to quantify the fluorescence response of neurons under different force levels, and to find a threshold under which no significant fluorescence response is displayed (the threshold force level to activate the class III ddaA neuron). Finally, we applied a touch force of 2 mN to the control group. This experiment was also performed for 30 times. This was to verify that the control group was unable to display significant change in fluorescence intensity even under the highest force level. The interval between each touch stimulation was set to be at least 1 min, which is long enough (>10 s) to allow the larva to completely recover from each stimulation [39].

During each stimulation, the fluorescence images of the neuron were collected at 8 fps. Fig. 6 shows typical image sequences of the GCaMP6 and RFP signals of the class III ddaA neurons of two larvae, from the experimental and control groups (touch force: 1 mN). The GCaMP6 signal increased upon touch and then gradually decreased to its baseline level after the stimulus was removed. Note that it may not be obvious to visually identify the touch-induced GCaMP6 signal change on the image sequence. The intensities of the GCaMP6 and RFP signals were quantified by calculating the average grayscale value of a 5 μm $\times$ 5 μm block that contains the major portion of the neuron ("area of interest" shown in Fig. 6). Denote the measured GCaMP6 and RFP intensities by F_{GCaMP6} and F_{RFP}, respectively. Using F_{RFP} as the reference, the normalized intensity $F_n = \frac{F_{GCaMP6}}{F_{RFP}}$. The relative increase of the normalized GCaMP6 intensity, $\frac{\Delta F_n}{F_n}$, was used to quantify the neuron response to a touch stimulus.

A. Independence of Neuronal Response to Repeated Stimulations

To illustrate that the neuron's response to each mechanical stimulation is independent, one class III ddaA neuron of a *Drosophila* larva from the experimental group was selected. A mechanical stimulus of 1 mN was applied to the same neuron for five times with a time interval of at least 1 min between each touch. The relative increase in the normalized GCaMP6 intensity ($\frac{\Delta F_n}{F_n}$) of the class III ddaA neuron is plotted in Fig. 7(a). To demonstrate that the neuron response to repeated touches has no significant difference, a two-tailed *t*-test with equal variances (validated by p value of F-test: $p = 0.491 > 0.05$) was conducted to compare the $\frac{\Delta F_n}{F_n}$ peak values from the four consecutive touches after the first touch (Fig. 7(a)) and those from the six first-time touches at 1 mN on the three larvae of the experimental group. The $\frac{\Delta F_n}{F_n}$ peak values of the four consecutive touches and six first-time touches are measured to be 0.212 ± 0.0228 and 0.206 ± 0.0230, respectively. The p value from the two-tailed *t*-test was determined to be 0.499, which is much larger than the threshold $p = 0.05$. This confirms that the neuron response to repeated touch is not significantly different from that of first-time touch.

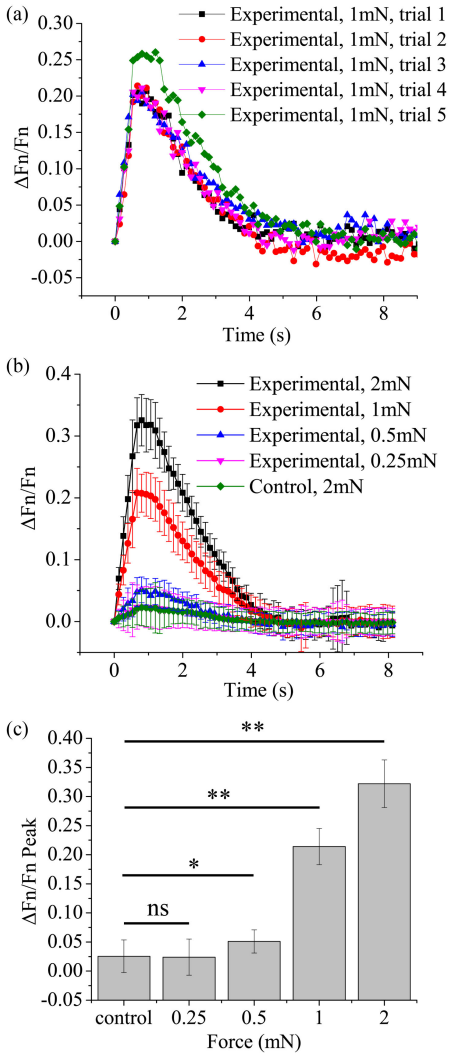

Fig. 7. (a) Comparison of responses to 1 mN mechanical stimuli five times on the same class III ddaA neuron. (b) Comparison of responses to mechanical stimuli of different force levels (n = 30). (c) peak response ($\frac{\Delta F_n}{F_n}$) under different mechanical stimulus. *: $p < 0.001$, **: $p < 0.0001$, and ns: not significant.

B. Responses to Touch Stimuli At Different Force Levels

The response of class III ddaA neurons to mechanical stimuli at different levels are plotted in Fig. 7(b). One can see that the larvae from the experimental group expressing NOMPC responded to the gentle touch, while the larvae from the control group without NOMPC expression did not show obvious response to gentle touch. For the experimental group, the peaks of $\frac{\Delta F_n}{F_n}$ in response to 2 mN, 1 mN, 0.5 mN and 0.25 mN are $32.2 \pm 4.1\%$, $21.4 \pm 3.1\%$, $5.1 \pm 2.0\%$ and $2.4 \pm 3.1\%$, respectively (n=30). For the control group, the peak of $\frac{\Delta F_n}{F_n}$ for 2 mN stimuli is $2.55 \pm 2.8\%$ (n = 30). We conducted pairwise comparison of the $\frac{\Delta F_n}{F_n}$ data from each experimental group and the control group using two-tailed *t*-test with equal or unequal variances based on *p* value from the F-test ($p_{control,\,0.25mN} = 0.3$, $p_{control,\,0.5mN} = 0.053$, $p_{control,\,1mN} = 0.303$, and $p_{control,\,2mN} = 0.028$) and the comparison results are shown in Fig. 7(c). The experimental group at 0.25 mN reveals no significant difference from the control group (*t*-test: $p = 0.872$), while the experimental groups at 0.5 mN, 1 mN, 2 mN show significantly higher $\frac{\Delta F_n}{F_n}$ peak values than the control group (*t*-test: $p_{control,\,0.5mN} = 0.00\,016$, $p_{control,\,1mN} = 9.63 \times 10^{-33}$, and $p_{control,\,2mN} = 1.66 \times 10^{-36}$, respectively). This indicates that the minimum force level required to trigger the response of the class III ddaA neuron is between 0.25 mN and 0.5 mN. To determine this threshold value, one needs to adopt a force sensor with much higher resolution than the one we adopted to accurately apply touch forces in the range of 0.25 mN and 0.5 mN with smaller differences, and also utilize a microscope lens with higher numerical aperture (thus higher resolution) for neuron fluorescence imaging. This will be investigated in our future study.

C. Discussion

The developed force controller combines the advantages of the fuzzy controller (fast convergence before reaching the threshold) and the compensation-prediction scheme (capability of handling force measurement noise, modeling errors, time delay, and insufficient feedback modality), and provides a good dynamic performance with a settling time of 0.15 s, zero overshoot and a force control resolution of <50 μN. The achieved high dynamic performance allows the system to replicate the sudden touch stimuli applied to *Drosophila* larvae during experiments [2]. Under a 1 mN stimulus, our system measured a 21.4% increase in the calcium fluorescence intensity of the class III ddaA neurons, which in good agreement with the previous results [2]. Furthermore, with the closed-loop force control capability and a control resolution better than 50 μN, we run the test under different force levels and decreased the applied force to as small as 0.25 mN. Quantitative relationship between the applied force level and the change in calcium fluorescence signal was acquired for the first time. The threshold force level at which the neuron started to get activated was determined to be in the range of 0.25–0.5 mN. Our experimental results demonstrate strong correlation between the neuronal activities and the applied force level [2]. The quantitative relationship between the fluorescence change and the force level suggests that the larva may display no danger-escaping behavior at a stimulus below 0.25 mN. This was not revealed in previous studies because of the lack of force control capability at the level below 1 mN [1]. In addition, compared to the previous work [31], the fluorescence image was taken at a higher frame rate without sacrificing the image quality by using the fluorescence camera, which enables the more accurate fluorescence measurement.

VI. Conclusion

This letter reported a robotic micromanipulation system for force-controlled touch stimulation and single-neuron fluorescence imaging of *Drosophila* larvae. Different force levels were accurately controlled by an advanced force controller. The teleoperated touching and imaging procedure alleviated the workload for a system operator. The combination of the switched fuzzy-PID controller and the compensation-prediction scheme successfully addressed challenges such as measurement noise,

modeling error, time delay and insufficient feedback modality altogether, providing fast convergence of force control both before and after reaching the switching threshold. Settling time and overshoot have been both reduced. The quantitative relationship between the calcium fluorescence change and the force level was experimental determined. The threshold above which the neuron started to respond to the stimulus was determined to be in the range of 0.25–0.5 mN. This system enables accurate mechanical stimulation of *Drosophila* larvae, which may lead to novel biological discoveries in the mechanotrasduction mechanisms of *Drosophila* larvae.

REFERENCES

[1] Y. Zhou, S. Cameron, W.-T. Chang, and Y. Rao, "Control of directional change after mechanical stimulation in drosophila," *Mol. Brain*, vol. 5, no. 1, pp. 39–51, 2012.

[2] A. Tsubouchi, J. C. Caldwell, and W. D. Tracey, "Dendritic filopodia, ripped pocket, nompc, and nmdars contribute to the sense of touch in drosophila larvae," *Curr. Biol.*, vol. 22, no. 22, pp. 2124–2134, 2012.

[3] P. Pan *et al.*, "Robotic stimulation of freely moving drosophila larvae using a 3d-printed micro force sensor," *IEEE Sens. J.*, vol. 19, no. 8, pp. 3165–3173, Apr. 2018.

[4] R. Y. Hwang *et al.*, "Nociceptive neurons protect drosophila larvae from parasitoid wasps," *Curr. Biol.*, vol. 17, no. 24, pp. 2105–2116, 2007.

[5] Y. Gao, J. Broussard, A. Haque, A. Revzin, and T. Lin, "Functional imaging of neuron-astrocyte interactions in a compartmentalized microfluidic device," *Microsyst. Nanoeng.*, vol. 2, no. 1, pp. 1–9, 2016.

[6] Y. Xiang, Q. Yuan, N. Vogt, L. L. Looger, L. Y. Jan, and Y. N. Jan, "Light-avoidance-mediating photoreceptors tile the drosophila larval body wall," *Nature*, vol. 468, no. 7326, pp. 921–928, 2010.

[7] Q. Yuan, Y. Xiang, Z. Yan, C. Han, L. Y. Jan, and Y. N. Jan, "Light-induced structural and functional plasticity in drosophila larval visual system," *Science*, vol. 333, no. 6048, pp. 1458–1462, 2011.

[8] W. Zhang, Z. Yan, L. Y. Jan, and Y. N. Jan, "Sound response mediated by the trp channels nompc, nanchung, and inactive in chordotonal organs of drosophila larvae," *Proc. Nat. Acad. of Sci.*, vol. 110, no. 33, pp. 13612–13617, 2013.

[9] Z. Yan *et al.*, "Drosophila nompc is a mechanotransduction channel subunit for gentle-touch sensation," *Nature*, vol. 493, no. 7431, pp. 221–225, 2013.

[10] R. Krenger, J. T. Burri, T. Lehnert, B. J. Nelson, and M. A. Gijs, "Force microscopy of the caenorhabditis elegans embryonic eggshell," *Microsyst. Nanoeng.*, vol. 6, no. 1, pp. 1–11, 2020.

[11] Y. Wei and Q. Xu, "Design and testing of a new force-sensing cell microinjector based on soft flexure mechanism," *IEEE Sens. J.*, vol. 19, no. 15, pp. 6012–6019, 2019.

[12] X. Liu, Y. Sun, W. Wang, and B. M. Lansdorp, "Vision-based cellular force measurement using an elastic microfabricated device," *J. Micromech. Microeng.*, vol. 17, no. 7, 2007, Art. no. 1281.

[13] X. Liu, K. Kim, Y. Zhang, and Y. Sun, "Nanonewton force sensing and control in microrobotic cell manipulation," *Int. J. Robot. Res.*, vol. 28, no. 8, pp. 1065–1076, 2009.

[14] J. Liu, J. Wen, Z. Zhang, H. Liu, and Y. Sun, "Voyage inside the cell: Microsystems and nanoengineering for intracellular measurement and manipulation," *Microsyst. Nanoeng.*, vol. 1, no. 1, pp. 1–15, 2015.

[15] S. Hu and D. Sun, "Automatic transportation of biological cells with a robot-tweezer manipulation system," *Int. J. Robot. Res.*, vol. 30, no. 14, pp. 1681–1694, 2011.

[16] C. C. Cheah, X. Li, X. Yan, and D. Sun, "Observer-based optical manipulation of biological cells with robotic tweezers," *IEEE Trans. Robot.*, vol. 30, no. 1, pp. 68–80, Feb. 2013.

[17] A. Thakur, S. Chowdhury, P. Švec, C. Wang, W. Losert, and S. K. Gupta, "Indirect pushing based automated micromanipulation of biological cells using optical tweezers," *Int. J. Robot. Res.*, vol. 33, no. 8, pp. 1098–1111, 2014.

[18] K. Kim, X. Liu, Y. Zhang, and Y. Sun, "Nanonewton force-controlled manipulation of biological cells using a monolithic mems microgripper with two-axis force feedback," *J. Micromech. Microeng.*, vol. 18, no. 5, 2008, Art. no. 0 55013.

[19] T. Tanikawa and T. Arai, "Development of a micro-manipulation system having a two-fingered micro-hand," *IEEE Trans. Robot. Automat.*, vol. 15, no. 1, pp. 152–162, 1999.

[20] M. Jeannerod, M. A. Arbib, G. Rizzolatti, and H. Sakata, "Grasping objects: The cortical mechanisms of visuomotor transformation," *Trends Neurosci.*, vol. 18, no. 7, pp. 314–320, 1995.

[21] S. Chowdhury, A. Thakur, C. Wang, P. Svec, W. Losert, and S. K. Gupta, "Automated indirect transport of biological cells with optical tweezers using planar gripper formations," in *Proc. IEEE Int. Conf. Automat. Sci. Eng.*, 2012, pp. 267–272.

[22] X. Liu, Z. Lu, and Y. Sun, "Orientation control of biological cells under inverted microscopy," *IEEE/ASME Trans. Mechatronics*, vol. 16, no. 5, pp. 918–924, Oct. 2010.

[23] C. Leung, Z. Lu, X. P. Zhang, and Y. Sun, "Three-dimensional rotation of mouse embryos," *IEEE Trans. Biomed. Eng.*, vol. 59, no. 4, pp. 1049–1056, Apr. 2012.

[24] W. Wang, X. Liu, D. Gelinas, B. Ciruna, and Y. Sun, "A fully automated robotic system for microinjection of zebrafish embryos," *PLoS One*, vol. 2, no. 9, 2007, Art. no. e 862.

[25] H. B. Huang, D. Sun, J. K. Mills, and S. H. Cheng, "Robotic cell injection system with position and force control: Toward automatic batch biomanipulation," *IEEE Trans. Robot.*, vol. 25, no. 3, pp. 727–737, 2009.

[26] W. H. Wang, X. Y. Liu, and Y. Sun, "High-throughput automated injection of individual biological cells," *IEEE Trans. Automat. Sci. Eng.*, vol. 6, no. 2, pp. 209–219, Apr. 2009.

[27] X. Liu *et al.*, "Automated microinjection of recombinant bcl-x into mouse zygotes enhances embryo development," *PLoS One*, vol. 6, no. 7, 2011, Art. no. e 21687.

[28] S. Zhuang *et al.*, "Visual servoed three-dimensional rotation control in zebrafish larva heart microinjection system," *IEEE Trans. Biomed. Eng.*, vol. 65, no. 1, pp. 64–73, Jan. 2017.

[29] S. Zhuang *et al.*, "Visual detection and two-dimensional rotation control in zebrafish larva heart microinjection," *IEEE/ASME Trans. Mechatronics*, vol. 22, no. 5, pp. 2003–2012, Oct. 2017.

[30] Z. Lu, X. Zhang, C. Leung, N. Esfandiari, R. F. Casper, and Y. Sun, "Robotic ICSI (intracytoplasmic sperm injection)," *IEEE Trans. Biomed. Eng.*, vol. 58, no. 7, pp. 2102–2108, Jul. 2011.

[31] W. Zhang, A. Sobolevski, B. Li, Y. Rao, and X. Liu, "An automated force-controlled robotic micromanipulation system for mechanotransduction studies of drosophila larvae," *IEEE Trans. Automat. Sci. Eng.*, vol. 13, no. 2, pp. 789–797, Apr. 2016.

[32] W. Zhang, X. Dong, and X. Liu, "Switched fuzzy-pd control of contact forces in robotic microbiomanipulation," *IEEE Trans. Biomed. Eng.*, vol. 64, no. 5, pp. 1169–1177, May 2017.

[33] W. Zhang, J. Qu, X. Zhang, and X. Liu, "A model compensation-prediction scheme for control of micromanipulation systems with a single feedback loop," *IEEE/ASME Trans. Mechatronics*, vol. 22, no. 5, pp. 1973–1982, Oct. 2017.

[34] X. Wang, Z. Chen, and G. Yang, "Finite-time-convergent differentiator based on singular perturbation technique," *IEEE Trans. Autom. Control*, vol. 52, no. 9, pp. 1731–1737, Sep. 2007.

[35] S. Fye, K. Dolma, M. J. Kang, and S. Gunawardena, "Visualization of larval segmental nerves in 3rd instar drosophila larval preparations," *J. Vis. Exp.: JoVE*, vol. 29, no. 43, 2010, Art. no. 2128.

[36] J. Betschinger, K. Mechtler, and J. A. Knoblich, "Asymmetric segregation of the tumor suppressor brat regulates self-renewal in drosophila neural stem cells," *Cell*, vol. 124, no. 6, pp. 1241–1253, 2006.

[37] B. Bello, H. Reichert, and F. Hirth, "The brain tumor gene negatively regulates neural progenitor cell proliferation in the larval central brain of drosophila," *Development*, vol. 133, no. 14, pp. 2639–2648, 2006.

[38] A. Pauli *et al.*, "Cell-type-specific TEV protease cleavage reveals cohesin functions in drosophila neurons," *Devlop. Cell*, vol. 14, no. 2, pp. 239–251, 2008.

[39] Y. Hu, Z. Wang, T. Liu, and W. Zhang, "Piezo-like gene regulates locomotion in drosophila larvae," *Cell Rep.*, vol. 26, no. 6, pp. 1369–1377, 2019.